Analysis of Baroque Sculpture Based on X-Ray Fluorescence Imaging and X-ray Computed Tomography Data Fusion

Daniel Vavřík[1], Ivana Kumpová[1], Michal Vopálenský[1], Jiří Lautenkranc[2]

[1]Institute of Theoretical and Applied Mechanics, Centre of Excellence Telč, Academy of Sciences of the Czech Republic, Batelovská 485, 588 56 Telč, Czech Republic, e-mail: vavrik@itam.cas.cz
[2]Artrestauro, Prague, Czech Republic

Abstract
It is advantageous to combine information about geometry and the inner structure of historical artifacts with information about the elemental composition of decorative layers, typically covering historical wooden sculptures. X-ray computed tomography describing artifact structure is quite common and easy. Standard X-ray fluorescence (XRF) analysis of decorative layers is typically done for several selected spots of the artifact's surface utilizing single pad detector. XRF imaging fully describing the surface's elemental composition is commonly done for flat objects, while time consuming XRF tomography is applied to relatively small objects. It will be shown in this work that an effective fusion combination of XRF imaging and X-ray tomography describing the whole object can be realized even when using a limited number of XRF images.

Keywords: X-ray Computed Tomography, X-ray Flourescence Imaging, Culutral Herritage, Data fusion

1. Summary

It is well known that the non-destructive X-ray computed tomography (XCT) of cultural heritage artifacts is advantageous for a number of reasons – documentation of the inner structure (damaging), preparation for restoration, dating, investigation of the manufacturing technology used [1], etc. In addition, many historical artifacts are covered by thin decorative layers for which evaluation of the elemental composition is important [2].

Mapping of the elemental composition of the artifact's surface layer is routinely performed utilizing the X-ray fluorescence (XRF) technique. Such mapping can be done employing a focused X-ray (or pencil beam) and a spectroscopic single pad detector where the investigated area is scanned. This technique is typical for the analysis of paintings, and it can be combined with X-ray radiography [3] or laminography. Another possible solution is using XRF computed tomography (XRF CT). This method requires a large number of XRF images to be recorded utilizing an XRF. Therefore, an intensive X-ray beam and a very small distance between the camera and the object studied are necessary to reduce the measuring time. This leads to restriction that only small objects can be studied. The XRF CT data obtained can easily be combined with standard XCT data [4], [5].

Instr Fig. 1. The Pieta wooden baroque sculpture is 600 mm high.

Another possible approach, which is especially advantageous for polychromed wooden sculptures, is proposed in this work. Historical wooden polychromed sculptures have typically been renovated several times during their existence. Such restoration work has usually been accompanied by the application of additive color layers. Therefore, one can assume that obtaining an overview of the surface layers elemental composition can be advantageous. Polychromes are typically typically composed from

several layers as for instance basic white color layer containing zinc or led which is silvered or golded. Related metal foil is usually covered by several color layers which can contain pigments based on other metals like iron, mercury, copper etc. Transparent varnish is typically used as final polychrome layer. Note that these decorative layers are relatively thin in comparison with sculpture dimensions, therefore XRF signal can be expected from the sculpture surface only as it is extremely low probability that XRF photons will transmitte through the investigated body.

The above-mentioned XRF CT and XCT data fusion is hardly applicable for wooden sculptures as these are usually quite big and geometrically complicated. Consequently, the distance between the XRF camera and the object studied has to be relatively large. This leads to the long measuring time necessary to create a single XRF image. Note that hundreds of such images are necessary for typical CT reconstruction. Such an obstacle can be overcome by combining XCT with several XRF images, where the XRF images are mapped onto an XCT volume. This data fusion will be demonstrated on a baroque carved wooden polychromed and silvered Pieta sculpture, which is richly decorated. See Fig. 1 for its photography. This Pieta was made in the 17th century in Bohemia. The sitting Virgin supports Christ on her lap. She wears a long veil covering a blue (originally red) pleated dress that falls to her feet. Christ is simply wearing his loincloth. Several samples from the Mary body were taken for chemical analysis (another analysis modality). It can be supposed on the basis of chemical analysis that an XRF signal of iron, zinc, silver, lead and mercury can primarily be expected. This paper is continuation of the work presented in [6].

2. Instrumentation

The Twinned Orthogonal Adjustable Tomograph (TORATOM) [7], utilized for XCT and XRF measurement has the capability to meet variable requirements regarding different radiographic and tomographic measurements, for instance the 2D scanning of leratively large samples as well as standard, dual-source [8] or dual-energy tomography [9] in different magnifications. TORATOM consists of two independent X-ray imaging lines in an orthogonal arrangement, with a shared rotational stage (Aerotech). TORATOM is equipped with 160 kV nanofocus and 240 kV microfocus tubes (X-RAY WorX GmbH). Detector holders allow the quick and easy replacement of the desired type of detector, Perkin Elmer flat panel with a 400 x 400 mm area and 200 μm pixel pitch was used in this work for CT measuerement. Two disc filter holders are employed for the beam hardening correction (BHC) method [10], [11] and for X-ray spectra shaping. The TORATOM components are positioned by a multi-axial computer-controlled system with absolute measuring system allowing recall already stored position of all components.

The gamma/XRF camera (XRF camera hereafter) used in this work has 100 μm pinhole and it is equipped with two stacked Timepix detectors. The pixelated Timepix detector [12] controlled by Pixelman software [13] can be operated in time-over-threshold mode (ToT), which enables measuring the energy of each incident photon [14], utilizing single event analysis [15]. One of the possible applications of this detector is XRF imaging [16]. Front detector of the XRF camera has a 300 μm thick silicon sensor, and the back detector has a 1 mm thick CdTe sensor. The XRF camera communicates via a USB 2.0 interface with maximal frame rate 30 fps. XRF imaging supposes a limited number of recorded photons per single frame to avoid pile ups. Installation of the camera in the TORATOM is depicted in Fig. 2. The flat panel behind the sculpture was utilized for the CT measurement employing a 160 kV nanofocus tube. The XRF camera on the left is a recording signal induced by the 240 kV tube (behind the XRF camera in this picture).

Figure. 2. The Pieta installed on the rotational table in the CT/XRF setup.

3. Mapping of XRF images onto surface of the object tomographically reconstructed

The principles of XRF imaging is depicted in Fig. 3. The XRF photons are detected by the XRF camera detector through a pinhole collimator of the camera (camera obscura imaging). XRF image resolution depends on the pinhole diameter, as a smaller pinhole leads to a higher resolution but to lower camera efficiency and vice versa. It has to be emphasized that an XRF image represents the projections of all XRF photons into an XRF detector plane, e.g. that no information about an object's 3D geometry is included in the XRF image. Magnification of the XRF image depends on the ratio between the distances "XRF camera pinhole – focal plane /XRF camera pinhole – camera detector". One consequence is that XRF image pixels may represent various areas as the object is generally 3-dimensional (i.e. we have various local magnifications). Therefore direct interpretation of the relation between the XRF image and a visual image of the object can be confusing.

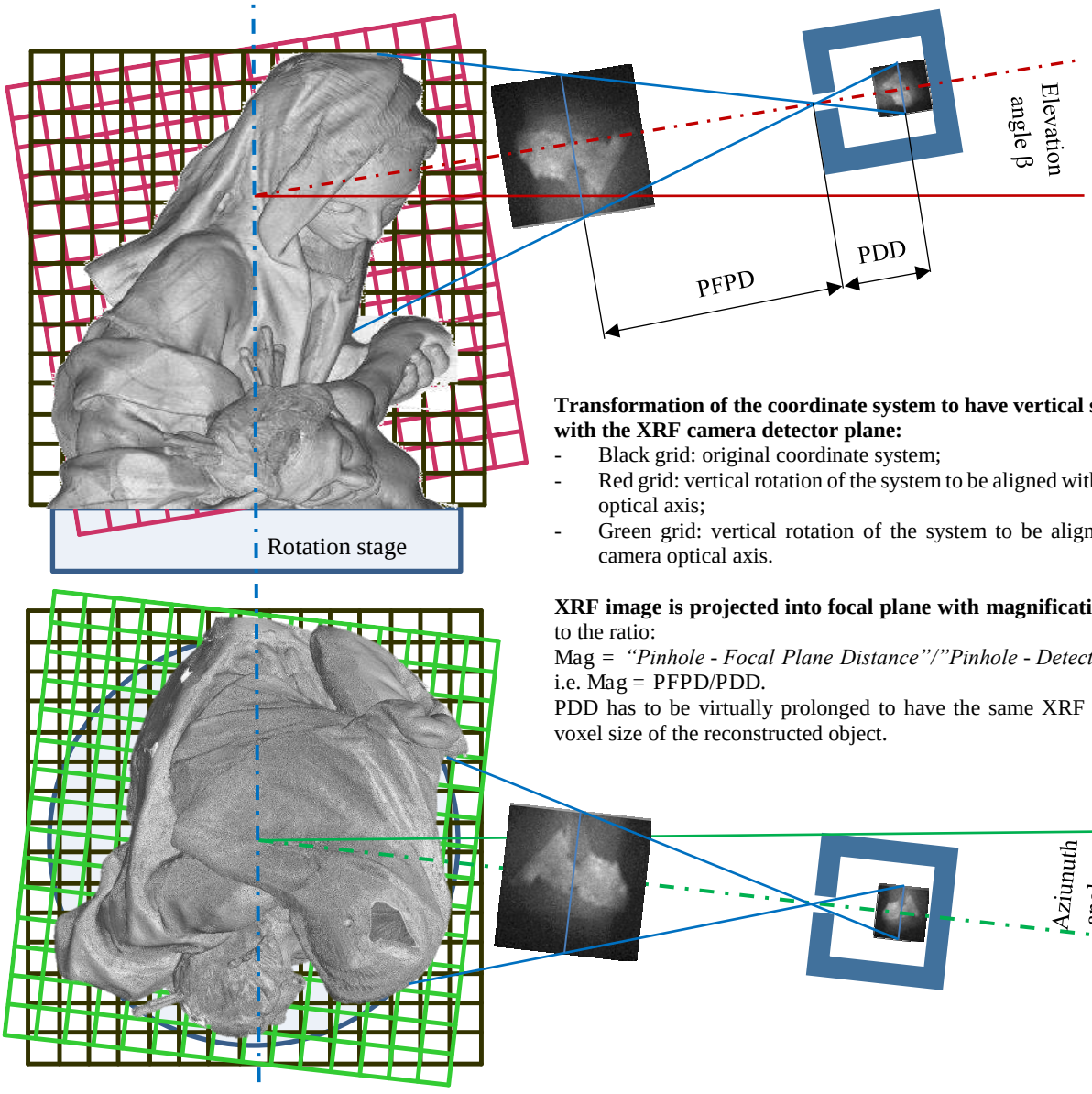

Transformation of the coordinate system to have vertical slices parallel with the XRF camera detector plane:

- Black grid: original coordinate system;
- Red grid: vertical rotation of the system to be aligned with XRF camera optical axis;
- Green grid: vertical rotation of the system to be aligned with XRF camera optical axis.

XRF image is projected into focal plane with magnification Mag equal to the ratio:
Mag = *"Pinhole - Focal Plane Distance"/"Pinhole - Detector Distance"*, i.e. Mag = PFPD/PDD.
PDD has to be virtually prolonged to have the same XRF pixel pitch as voxel size of the reconstructed object.

Figure 3. The principle of the XRF imaging and mapping.

Any image can be mapped onto virtual model surface if this surface is mathematically described (common task for virtual reality for instance). For tomographic reconstruction for instance, isosurface corresponding to the object boundaries are triangulized and the image is mapped onto each triangle with respect of its spatial orientation. One triangle can be exptremelly small if the object has tinny details. Such approach is highly demanding for programming and related calcualations. Fortunatelly quite simple solution which is effective and easy to program was found. The related software was developed in Matlab enviroment (MathWork).

The XRF data were mapped into surface layer of the reconstructed object as follows :

1. The coordination system of the volume is transformed to have vertical slices parallel with the XRF camera detector, this operation is illustrated in Fig.3.
2. Desired energy channels are selected from the full XRF image. Three channels named R, G and B (regarding to the RGB image coding) are used in this work. Next steps describing XRF mapping are done for all three energy channels succesivelly, i.e. three new volumes are generated.
3. The vertical slice nearest to the XRF camera is selected. Two auxiliary "slices" are generated: first one is positive binarized vertical slice (hereafter positiv), i.e. a value of 1 is written into voxels which have a value higher than the given threshold (corresponding to air) and a value of 0 is written into voxels with a value lower than the same threshold; second one is negative binarized slice (hereafter negativ), which is inverze to the positive slice.
4. XRF image is magnified regarding to the position of the vertical slice. Data are interpolated to have the same position of the XRF image pixels as voxels of the selected slice.
5. The positiv is multiplied with the energy channel of the XRF image, resultant image is recorded into related volume slice.
6. The negativ is multiplied with the XRF channel, i.e. value of the XRF pixels are set to zero when value 1 of the positiv was met. This solution ensure that data from XRF are not not written into other voxels laying behind the first detected material.
7. Operations described in points 3-6 are repeated for other slices in successively from the second slice nearest to the XRF camera up to the slice furthest from the camera.

4. Experimental

As the studied sculpture is relatively tall (600 mm), only its top half was scanned during the CT measurement with the following parameters: nanofocus tube at 160 kVp and 20 W on the target; 5 μm spot size; 1200 projections with 1 s exposure; Perkin Elmer flat panel detector (0.2 mm pixel pitch). The tube focus-detector distance (FDD) was 1260 mm, and the focus-object distance (FOD) was 1022 mm. The voxel size was consequently 0.162 mm. An example of the CT visualization is depicted in Fig. 4. Reconstruction and visualziation was done employing VGstudio Max 3.0 (Volume graphics). It was proven that sculpture was made from one masive wood piece, where only two other small parts were added. Polychrome layers are manifested as white contour surrounding sculpture body in tomographic crossections.

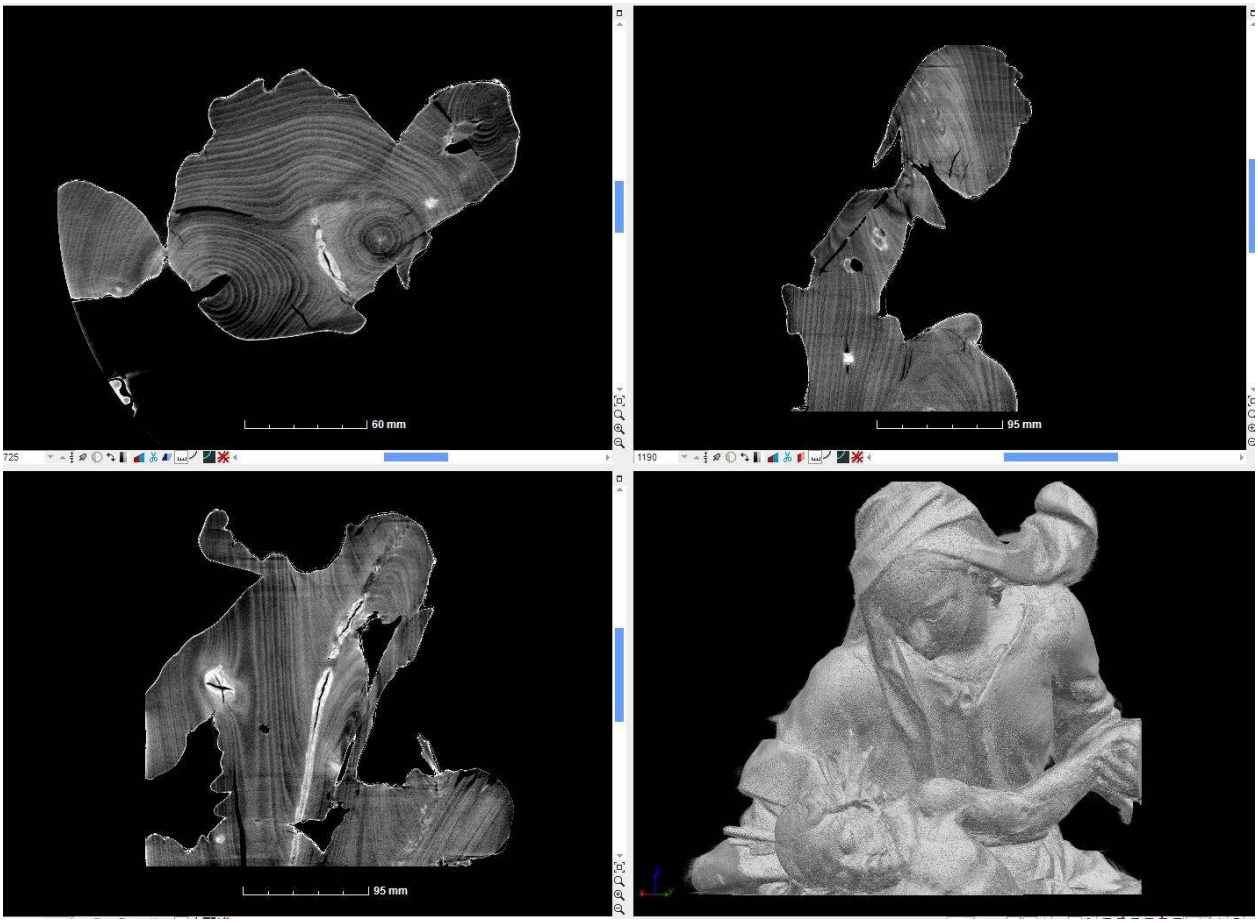

Figure 4: Visualization of the reconstructed Pieta. Wooden structure is well visible. Polychrome layer covering sculpture, which has a higher density than wood, is manifested as white-black contour surounding crossections.

The XRF camera was installed with a 54˚ azimuth from the X-ray beam axis of the 160 kV tube (used for CT data acquisition) and a 5˚ elevation angle from the horizontal plane. Other XRF data were taken with azimuth 54˚ and 24º respectivelly. Related 240 kV microfocus tube was operated at 110 kVp and 100 W on the target. The XRF data were recorded at a 13 fps frame rate and an exposure time of 5 ms per single frame (plus a 2.64 ms read-out time). In total, $15x10^3$ frames were recorded within 19 minutes for a single XRF image. The recorded images were analyzed utilizing single event analysis [15]. XRF images taken from three azimuth angles are depicted in Fig. 5. RGB coding of these images is based on the energy channels where each one is covering specific energy window related with three identified basic materials – iron, zinc and silver.

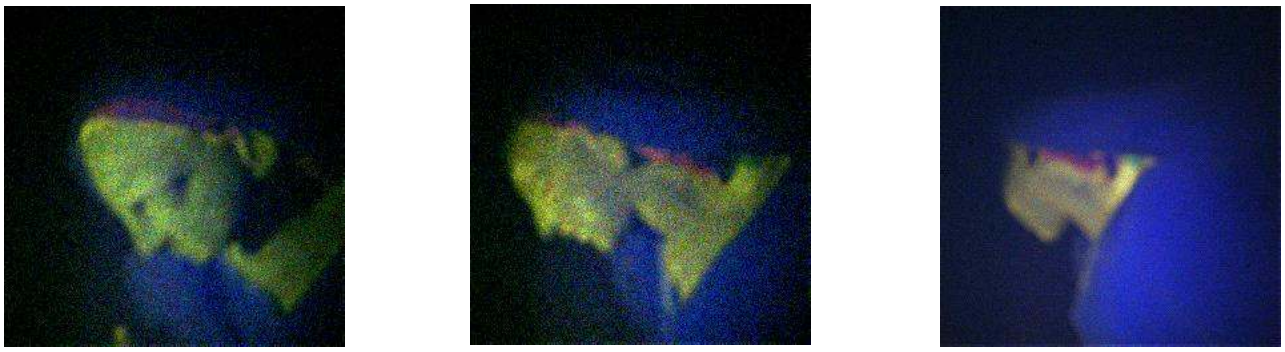

Figure 5. XRF image in the RGB representation. Left one was taken with azimuth angle 84 º, middle image with azimuth 54˚ and right one with azimuth 24º respectivelly. The mixture of materials is expressed by the resultant color: R 3-7 keV (covering iron XRF peak), G 8-16keV (zinc), B 18-28keV (silver and scattered photons).

The mapping procedure is illustrated in Fig. 6 for XRF image taken from 54˚ azimuth for the XRF images represent total signal without any energy information. First subimage top left represents situation where focal plane is not in the contact with the reconstructed volume. Other focal planes are crossing the reconstructred volume while XRF images are successively enlarged regarding to the related magnificatin. Depicted focal planes have 32.4 mm pitch.

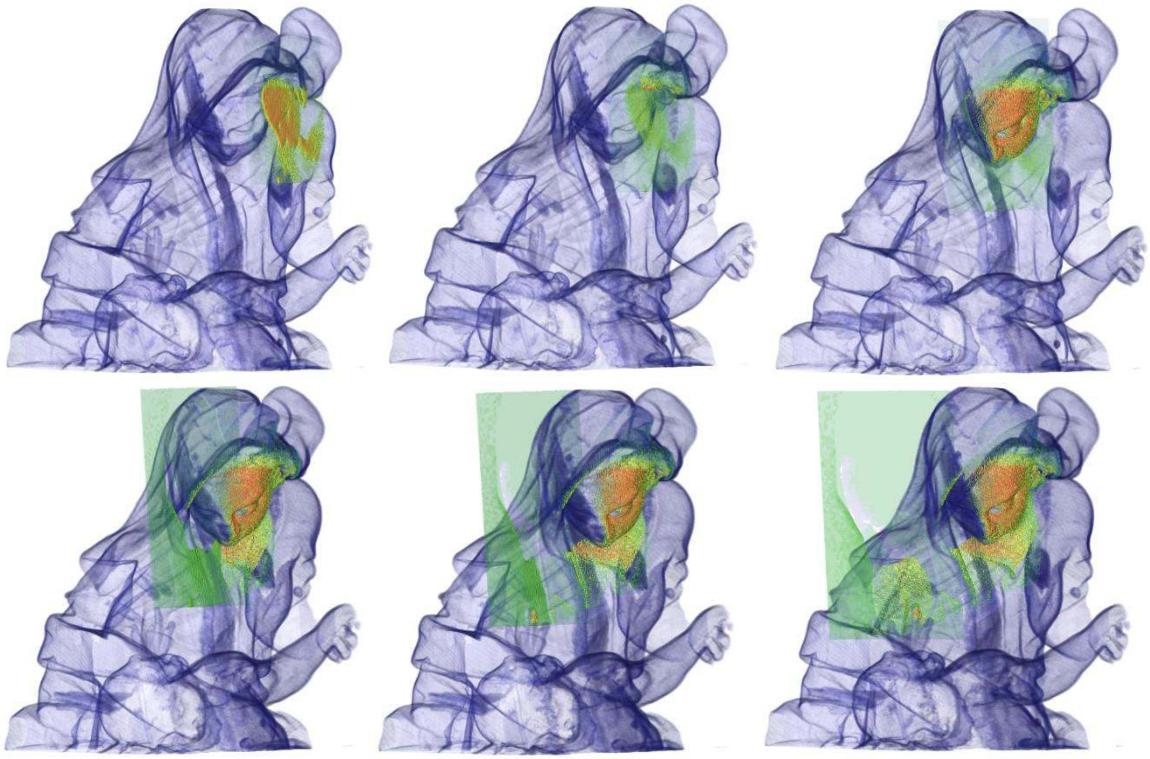

Fig. 6: Mapping of the XRF signal taken at 60˚ azimuth angle, depicted focusing planes have 32.4 mm pitch.

Mapping of all energy channels for three measured azimut angles is depicted in Fig. 7 utilizing RGB coding. Only Piete head is imaged to show relations with XRF images in Figure 5. It is visible that mapped and original XRF images looks similar, however mapped images have different shape due to 3D geometry of the Pieta (see bottom edge of the mapped image for instance).

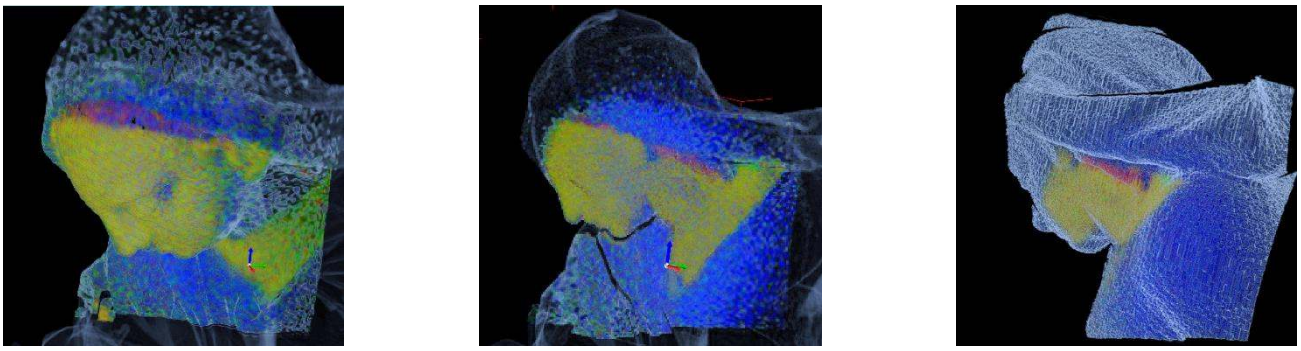

Figure 7: XRF images from all three angles mapped onto tomographic reconstruction. Colors represent energy the same energy windows as utilized for Fig. 5.

Whole CT reconstruction with mapped XRF image for azimuth angle 84° is depicted in Fig. 8 left. Reconstructed volume where XRF images from all three measured azimuth angles were mapped is shown in Fig. 8 right. Note, that although Pieta is much better covered by the XRF signal, some areas are still not desribed . It leads to the conclusion that other elevations and azimuth angles should be applied.

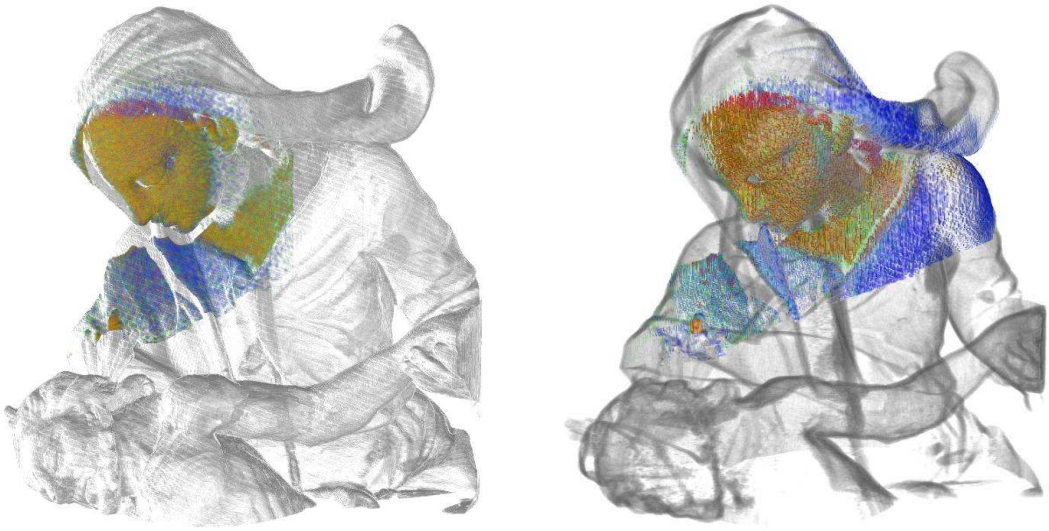

Figure 8: XRF images from all three angles mapped onto tomographic reconstruction. Colors represent energy the same energy windows as utilized for Fig. 5.

5. Conclusions

It was proven that the fusion of XRF imaging and CT helps to identify the distribution of the various elements and relationships between the surface's material composition and the geometry of the reconstructed volume. It is relatively easy to implemen proposed method of the XRF mapping into surface layer of the CT volume.

It was estimated that only 9 XRF images taken during one rotation would be enough to cover the Pieta's head fully,.although XRF signal can be still missed for some areas. Additive azimuth and elevatin angles can solve this problem excpept of deeply concave areas. Neverthless, time needed for XRF data acquisition for whole scuplture would be still rasonable.

Acquisition of XRF images with better statistics has to be done for better material identificaion/imaging. New generation of the detector which will be used for future work has better energy resolution and higher frame rate (i.e. better statistic with the same acqusition time).

Acknowledgment

The research was supported by Project No. DG16P02M022 of the Applied Research and Development of National and Cultural Identity Programme and by the project No. LO1219 under the National sustainability programme I of the Ministry of Education, Youth and Sports of the Czech Republic.

References

[1] Berg, Ina. Looking through pots: recent advances in ceramics X-radiography. Journal of Archaeological Science [online]. 2008, vol. 35, no. 5, pp. 1177–1188

[2] Papadopoulou, D., et al. Study of decorated archeological ceramics by micro X-ray fluorescence spectroscopy. NIM A, 2007, vol. 580, no. 1, pp. 743–746

[3] Matthias Alfeld, et al., Optimization of mobile scanning macro-XRF systems for the in situ investigation of historical paintings, J. Anal. At. Spectrom. 2011, DOI: 10.1039/C0JA00257G.

[4] C. Hall, Combined X-ray fluorescence and absorption computed tomography using a synchrotron beam, JINST 8 C06007, 2013, doi:10.1088/1748-0221/8/06/C06007.

[5] D. Hampai, et al., X-Ray micro-computed tomography and micro X-ray fluorescence mapping of synthetic emerald by using a laboratory polycapillary optics X-ray tube layout, X-Ray Spectrometry, 2015, X-Ray Spectrometry, doi. 10.1002/xrs.2600.

[6] D. Vavrik et al.: Multimodal Analysis of Cultural Heritage Artefacts Utilizing Computed Tomography and X-Ray Fluorescence Imaging, will be published In. IEEE Nuclear Science Symposium Conference Record, 2016

[7] T. Fila, D. Vavrik. A multi-axial apparatus for carrying out x-ray measurements, particularly computed tomography. European patent EP2835631. Granted 24.02.2016.

[8] Fila, T.; et al., Utilization of dual-source X-ray tomography for reduction of scanning time of wooden samples. Journal of Instrumentation. 2015, Vol. 10, No. 5, C05008. ISSN 1748-0221.

[9] Fila, T., et al., Dual-energy X-ray micro-CT imaging of hybrid Ni/Al open-cell foam, JINST C01005-C01005, (2016) doi. 10.1088/1748-0221/11/01/C01005.

[10] Vavrik, D.; Jakubek, J. Radiogram enhancement and linearization using the beam hardening correction method. Nuclear Instruments & Methods in Physics Research Section A. 2009, Vol. 607, pp. 212-214.

[11] J. Jakubek, Data processing and image reconstruction methods for pixel detectors, Nucl. Instrum. Meth. A 576 (2007) 223.

[12] Llopart X. et al., Timepix, a 56k programmable pixel readout chip for arrival time, energy and/or photon counting measurements, Nucl. Instrum. Meth. A 581 (2007) 485.

[13] T. Holy et al., Data acquisition and processing software package for Medipix2, Nucl. Instrum. Meth. A 563 (2006) 254.

[14] J. Jakubek, Precise energy calibration of pixel detector working in time-over-threshold mode, Nucl. Instrum. Meth. A 633 (2011) S262.

[15] T. Holy, et al., Pattern recognition of tracks induced by individual quanta of ionizing radiation in Medipix2 silicon detector, Nucl. Instrum. Meth. A 591, 287 (2008).http://dx.doi.org/10.1016/j.nima.2008.03.074

[16] Zemlicka, J., et al., Energy and position sensitive pixel detector Timepix for X-ray fluorescence imaging, Nucl. Instrum. Meth. A 607 (2009) 202.